

1 Determining the Plio-Quaternary uplift of the southern French massif-Central; a new insights for
2 intraplate orogen dynamics.

3

4 Oswald Malcles¹, Philippe Vernant¹, Jean Chéry¹, Pierre Camps¹, Gaël Cazes^{2,3}, Jean-François
5 Ritz¹, David Fink³.

6 ¹Geosciences Montpellier, CNRS-University of Montpellier, Montpellier, France

7 ²SEES, University of Wollongong, Wollongong, Australia

8 ³Australian Nuclear Science and Technology Organisation, Lucas Heights, Australia

9

10 *Correspondence to:* Oswald Malcles (oswald.malcles@umontpellier.fr)

11 **Abstract.**

12 The evolution of intra-plate orogens is still poorly understood. Yet, this is of major importance for
13 understanding the Earth and plate dynamics, as well as the link between surface and deep geodynamic
14 processes. The French Massif Central is an intraplate orogen with a mean elevation of 1000 m, with
15 the highest peak elevations ranging from 1500 m to 1885 m. However, active deformation of the
16 region is still debated due to scarce evidence either from geomorphological or geodetic and
17 seismologic data. We focus our study on the southern part of the Massif-Central, known as the
18 Cévennes and Grands Causses, which is a key area to study the relationship between the recent
19 geological deformation and landscape evolution. This can be done through the study of numerous
20 karst systems with trapped sediments combined with the analysis of a high-resolution DEM.

21 Using the ability of the karst to durably record morphological evolution, we first quantify the incision
22 rates. We then investigate tilting of geomorphological benchmarks by means of a high-resolution
23 DEM. We finally use the newly quantified incision rates to constrain numerical models and compare
24 the results with the geomorphometric study.

25 We show that absolute burial age (¹⁰Be/²⁶Al on quartz cobbles) and the paleomagnetic analysis of
26 karstic clay deposits for multiple cave system over a large elevation range correlate consistently. This
27 correlation indicates a regional incision rate of 83^{+17}_{-5} m/Ma during the last ca 4 Myrs (Pliocene-
28 Quaternary). Moreover, we point out through the analysis of 55 morphological benchmarks that the
29 studied region has undergone a regional southward tilting. This tilting is expected as being due to a
30 differential vertical motion between the north and southern part of the studied area.

31 Numerical models show that erosion-induced isostatic rebound can explain up to two-thirds of the
32 regional uplift deduced from the geochronological results and are consistent with the southward tilting
33 derived from morphological analysis. We presume that the remaining unexplained uplift is related to
34 dynamic topography or thermal isostasy due to the Massif Central Pliocene-Quaternary magmatism.

35 Integrating both geochronology and morphometrical results into lithospheric-scale numerical models
36 allows a better understanding of this intraplate-orogen evolution and dynamic. We assume that the
37 main conclusions are true to the general case of intraplate deformation. That is to say, once the
38 topography has been generated by a triggering process, rock-uplift is then enhanced by erosion and
39 isostatic adjustment leading to a significant accumulation of mainly vertical deformation.

40 **1 Introduction**

41 Since the past few decades, plate-boundary dynamic is, to a first order, well understood. This is not
42 the case for intraplate regions, where short-term (10^3 - 10^5 yr) regional strain rates are low and the
43 responsible dynamical processes are still in debate (e.g. Calais et al., 2010; Vernant et al., 2013; Calais
44 et al., 2016; Tarayoun et al., 2017). Intraplate deformations evidenced by seismic activity is
45 sometimes explained by a transient phenomenon (e.g., glacial isostatic rebound, hydrological
46 loading). However, to explain the persistence through time of intraplate deformation, and explain the
47 high finite deformation we can observe in the topography in many parts of the world as for instance
48 the Ural mountains in Russia, the Blue Mountains in Australia or the French Massif Central, one
49 needs to invoke continuous processes at the geological time-scale.

50 Located in the southwestern Eurasian plate (Fig. 1), the French Massif Central is an ideal case to
51 study this processes because a high resolution DEM encompasses the whole region and widespread
52 karstic areas are present along its southern and western edges, allowing the possibility to quantify
53 landscape evolution rates thanks to TCN burial ages. The region is characterized by a mean elevation
54 of 1000 m with summits higher than 1500 m. Such topography is likely to be the result of recent,
55 active uplift and as the Cevennes mountains experiences an exceptionally high mean annual rainfall
56 (the highest peak, Mount Aigoual, records the highest mean annual rainfall in France of 4015 mm) it
57 raises the question of a possible link between erosion and uplift as previously proposed for the Alps
58 (Champagnac et al., 2007; Vernant et al., 2013; Nocquet et al., 2016). This region currently undergoes
59 a small but discernible deformation, but no significant quantification can be deduced due to the
60 scarcity in seismicity (Manchuel et al., 2018). In addition, GPS velocities are below the uncertainty
61 threshold of GPS analyses (Nocquet et Calais, 2003; Nguyen et al., 2016).

62 In this study we focus on the Cevennes Mountains and the Grands Causses (Fig.1) area, where cave
63 systems with trapped sediments are known over a widespread altitude range. South and West of the
64 crystalline Cevennes mountains, prominent limestone plateaus, named Grands Causses, rise to 1000m
65 and are dissected by few canyons that are several hundreds of meter deep. The initiation of incision,
66 its duration and the geomorphic processes leading to the present-day landscape remain poorly
67 constrained. A better understanding of the processes responsible for this singular landscape would
68 bring valuable information on intraplate dynamics, especially where large relief exists.

69

70 **2. Geological background**

71 The oldest rock units in the study area were formed during the Variscan orogeny (late Palaeozoic,
72 ~300 Ma; Bricau et al., 2007) and constitute the crystalline basement of the Cevennes. Between 200
73 and 40 Ma (Mesozoic and middle Cenozoic), the region was mainly covered by the sea ensuring the
74 development of an important detrital and carbonate sedimentary cover, which can reach several km of
75 thickness in some locations (Sanchis and Séranne, 2000; Barbarand et al., 2001). During the Mesozoic
76 era, an episode of regional uplift and subsequent erosion and alteration (called the Durancian event) is
77 proposed for the origin of the flat, highly elevated surface that persists today across the landscape

78 (Bruxelles, 2001; Husson, 2014).

79 The area is affected by the major NE-SW trending Cevennes fault system, a lithospheric-scale fault,
80 inherited from the Variscan orogen. This fault system was reactivated several times (e.g. as a strike-
81 slip fault during the Pyrenean orogen or as a normal fault during the Oligocene extension). During the
82 Pyrenean orogeny, between 85 to 25 Ma (Tricart, 1984; Sibuet et al., 2004), several faults and folds
83 systems affected the geological formations south of the Cevennes fault, while very few deformations
84 occurred farther north within the Cévennes and Grand Causses areas (Arthaud and Laurent, 1995).
85 Finally, the Oligocene extension (~30 Ma) led to the counterclockwise rotation of the Corso-Sardinian
86 block and the opening of the Gulf of Lion, re-activating some of the older compressive structures as
87 normal faults. The main drainage divide between the Atlantic Ocean and the Mediterranean Sea is
88 located in our study area and is inherited from this extensional episode (Séranne et al., 1995; Sanchis
89 et al., 2000).

90 Afterwards during the Pliocene-Quaternary period, an intense volcanic activity has affected the
91 region, from the Massif Central to the Mediterranean shoreline. This activity is characterized by
92 several volcanic events that are well constrained in age (Dautria et al., 2010). The last eruption
93 occurred in the Chaîne des Puys during the Holocene (i.e. the past 10 kyrs (Nehlig et al., 2003;
94 Miallier et al., 2004). Some authors proposed that this activity is related to a hotspot underneath the
95 Massif Central leading to an observed positive heat-flow anomaly and a possible regional Pliocene-
96 Quaternary uplift (Granet et al., 1995; Baruol and Granet, 2002). Geological mapping at different
97 scale can be found at: <http://infoterre.brgm.fr/>.

98 Despite this well described overall geological evolution the onset of active incision that has shaped
99 the deep valleys and canyons (e. g. Tarn or Vis river, Fig 1) across the plateaus, and the mechanisms
100 that controlled this incision are still debated. One hypothesis proposes that canyon formation was
101 driven by the Messinian salinity crisis with a drop of more than 1000 m in Mediterranean Sea level
102 (Mocochain, 2007). This, however, would then not explain the fact that the Atlantic watersheds show
103 similar incision. Other studies have suggested that the incision is controlled by the collapse of cave
104 galleries that lead to fast canyon formation mostly during the late Quaternary, thus placing the onset
105 of canyon formation only a few hundreds of thousands of years ago (Corbel, 1954). More recently, it
106 has been proposed (based on relative dating techniques and sedimentary evidence) that incision
107 during the Quaternary was negligible (i.e. less than a few tens of meters), and that the regional
108 morphological structures seen today occurred around 10 Ma (Séranne et al., 2002; Camus, 2003).

109

110 **3. Materials and methods**

111 In this paper, we provide new quantitative constraints on both the timing of incision and the rate of
112 river down-cutting in the central part of the Cévennes and of the Grands Causses that has resulted in
113 the large relief between plateau and channel bed.

114 We employ two methods to infer allochthonous karstic infilling age and associated river down-
115 cutting. First, we use quartz cobbles to measure concentration of cosmogenic ^{10}Be and ^{26}Al isotopes.
116 The $^{10}\text{Be}/^{26}\text{Al}$ ratio provide burial ages of these karstic infilling. Second, paleomagnetic analyses of

117 clay deposits to obtain paleo-polarities. In both cases, vertical profiles among tiered caves systems
118 and horizontal galleries could provide local incision rate information. By analyzing a high-resolution
119 DEM (5m), we show that the region is affected by a southeastward regional tilting. Our results allow
120 to quantify the role of the Pliocene-Quaternary incision on the Cévennes landscape evolution and to
121 constrain numerical modeling from which we derive the regional uplift rates and a tilt of
122 geomorphological markers.

123 If incision is initiated by uplift centered on the North of the area where elevations are maximum, it
124 will lead to tilting of fossilized topographic markers as strath terraces. Our research approach provides
125 an opportunity to discriminate between three possible explanations for the current terrain morphology.
126 The first is based on old uplift and old incision (Fig. 2A). In this case, apparent incision rates would
127 be very low. For instance, if incision commenced 10 Ma (Serrane et al., 2002), we would find surface
128 tilting but cosmogenic burial dating with $^{10}\text{Be}/^{26}\text{Al}$ which cannot discern ages older than $\sim 5\text{Ma}$ due to
129 excessive decay of ^{26}Al , would not be possible. The second possibility (Fig. 2B) is that the uplift is
130 old, and incision consequently follows but with a time lag. Here the incision rate would be rather fast,
131 but no tilting is expected for the river-related markers because no differential uplift occurs after their
132 formation. Finally, the third possibility (Fig 2C) is that uplift and incision are concurrent and recent
133 (i.e. within the time scale of cosmogenic burial dating) and thus we would expect burial ages < 5
134 Myrs relatively high incision rates, and tilting of morphological markers. These different proposals for
135 the temporal evolution of the region will then be compared using numerical modeling.

136 **4. Determining the incision rates in the Cévennes and the Grand Causses Region**

137 **4.1. Principles and methods**

138 **4.1.1. Karst model**

139 No evidence of important aggradation events has been reported in the literature for the studied area.
140 Therefore, we base our analysis on a per descensum infill model of the karst networks whereby
141 sediments are transported and then deposited within cave galleries close to base level. When cave-
142 systems and entry passages are near the contemporaneous river channel elevation (including higher
143 levels during floods), the deposition into caves of sediments, from clay to cobbles occurs, especially
144 during flood events. Subsequent river incision into bedrock creates a relative base level drop (due to
145 uplift or sea-level variations). The galleries associated with the former base-level are now elevated
146 above the new river course and become disconnected from further deposition. Hence fossilised and
147 trapped sediments throughout the cave network represent the cumulative result of incision. In this
148 commonly used model (Granger et al., 1997; Audra et al., 2001; Stock et al., 2005; Harmand et al.,
149 2017), the higher the gallery elevation (relative to the present-day base level) the older the deposits in
150 that gallery. As a result, the objective here is to quantify a relative lowering of the base level in the
151 karst systems, with the sediments closest to the base level being the youngest deposits, and note that
152 we do not date the cave network creation which may very well pre-date river sediment deposition.

153 Within individual canyons, successions of gallery networks across the full elevation range from
154 plateau top to modern river channel, were not always present and often sampling could not be
155 conducted in a single vertical transect. Thus, we make the assumption of lateral altitudinal continuity
156 i.e. that within a watershed, which may contain a number of canyons, the sediments found in galleries
157 at the same elevation were deposited at the same time. Inside one gallery, we use the classical
158 principle of stratigraphy sequence (i.e. the older deposits are below the younger ones). More
159 informations and detailed relationships concerning the karstic development and geometric relationship
160 between karstic network and morphological markers could be find in Camus (2003). In any cases, our
161 aim is not to date the galleries formation, neither to explain the formation processes (e.g. past
162 preferential alteration layer); but to use the time information brought by the sediment that have been
163 trapped into the cave system. Therefore, we apply the common used model (example in Harmand et
164 al., 2017) that had been proved by Granger et al., (1997, 2001). For cave topographic survey, we refer
165 the reader to https://data.oreme.org/karst3d/karst3d_map that provides 3D survey.

166 **4.1.2. Burial ages**

167 Burial dating using Terrestrial cosmogenic nuclides (TCN) is nowadays a common tool to quantify
168 incision rates in karstic environment (Granger and Muzikar, 2001; Stock et al., 2005; Moccochain.,
169 2007; Tassy et al., 2013; Granger et al., 2015; Calvet et al., 2015; Genti, 2015; Olivetti et al., 2016;
170 Harmand et al., 2017; Rovey II et al., 2017; Rolland et al., 2017; Sartégou, 2017; Sartégou et al.,
171 2018). This method relies on the differential decay of TCN in detrital rocks that were previously
172 exposed to cosmic radiation before being trapped in the cave system. With this in mind, the ^{10}Be and
173 ^{26}Al nuclide pair is classically used as (i) both nuclides are produced in the same mineral (i.e. quartz),
174 (ii) their relative production ratio is relatively well constrained (we use a standard $^{26}\text{Al}/^{10}\text{Be}$ pre-burial
175 ratio of 6.75, see Balco et al., 2008) and (iii) their respective half-lives (about 1.39 Myr and 0.70 Myr
176 for ^{10}Be and ^{26}Al , respectively) are well suited to karstic and landscape evolution study, with a useful
177 time range of ~100 ky to ~5 Myr.

178 To quantify the incision rate of the limestone plateau of the Cevennes area, we analysed quartz
179 cobbles infilling from four caves of the Rieutord canyon (Fig. 1), this canyon is well suited for such
180 study because horizontal cave levels are tiers over 200 m above the current river-level and are directly
181 connected to the canyon, leading to a straight relationship between river elevation and the four cave
182 infilling that we have sampled (Cuillère cave, Route cave, Camp-de-Guerre cave and Dugou cave).
183 Furthermore, cobbles source is well known and identified: the upstream part of the Rieutord river,
184 some tens of kilometers northward, providing a unique sediment origin composed of granite and
185 metamorphic rocks embedding numerous quartz veins. All samples (Example Fig. 3) were collected
186 far enough away (>20m) from the cave entrance and deep enough below the surface (>30m) to avoid
187 secondary in-situ cosmogenic production of ^{10}Be and ^{26}Al in the buried sediments.

188 The quartz cobbles were first crushed and purified for their quartz fraction by means of sequential
189 acid attack with Aqua-Regia ($\text{HNO}_3 + 3\text{HCl}$) and diluted Hydrofluoric acid (HF). Samples were then

190 prepared according to ANSTO's protocol (see Child et al. 2000) and ~300µg of a ⁹Be carrier solution
191 was added to the purified quartz powder before total dissolution. AMS measurements were performed
192 on the 6MV SIRIUS AMS instrument at ANSTO and results were normalised to KN-5-2 (for Be, see
193 Nishiizumi et al., 2007) and KN-4-2 (for Al) standards. Uncertainties for the final ¹⁰Be and ²⁶Al
194 concentrations include AMS statistics, 2% (Be) and 3% (Al) standard reproducibility, 1% uncertainty
195 in the Be carrier solution concentration and 4% uncertainty in the natural Al measurement made by
196 ICP-OES, in quadrature. Sample-specific details and results are found in table 1.

197 **4.1.3. Paleomagnetic analysis**

198 In parallel with burial dating, we analyzed the paleomagnetic polarities within endokarstic clay
199 deposits within two main cave systems: the *Grotte-Exsurgence du Garrel* and the *Aven de la Leicasse*
200 (Fig. 1). These two cave systems allowed us collecting samples along a more continuous range of
201 elevations than the one provided by the Rieutord samples (for burial age determination) and also
202 extending the spatial coverage to the Southern Grands Causses region. Thanks to the geometry of
203 these two cave systems, we sampled a 400m downward base level variation. The sampling was done
204 along vertical profiles from a few ten of centimeters to 2 meters high by means of Plexiglas cubes
205 with a 2 cm edge length (Fig. 4) used as a pastry cutter. We weren't able to analyse clay samples from
206 Rieutord canyon because no reliable clay infilling was found in the Rieutord caves.

207 Demagnetisation was performed with an applied alternative field up to 150mT using a 2G-760
208 cryogenic magnetometer, equipped with the 2G-600 degausser system controller. Before this analysis,
209 each sample remained at least 48h in a null magnetic field, preventing a possible low coercivity
210 viscosity overprinting the detrital remanent magnetisation (DRM) (Hill, 1999; Stock et al., 2005;
211 Hajna et al., 2010). If the hypothesis of instantaneous locked in DRM seems reasonable compared
212 with the studied time span, it is important to keep in mind that the details of DRM processes (as for
213 instance the locked in time) is not well understood (Tauxe et al., 2006; Spassov et Valet, 2012) and
214 could possibly lead to small variations (few percents) in the following computed incision rates.

215 Because fine clay particles are expected being easily reworked in the cave, careful attention was paid
216 to the site selection and current active galleries were avoided. Clays deposits had to show well
217 laminated and horizontal layering in order to prevent analysis of in-situ produced clays (from
218 decalcification) or downward drainage by an underneath diversion gallery that could strongly affect
219 the obtained inclination (and also the declination to a minor extent). Note that for paleo-polarities
220 study alone, small inclination or declination variations won't result in false polarities

221 **4.2 Quantifying the average incision rates**

222 **4.2.1. Local incision rate from burial ages (Rieutord Canyon)**

223

224 The relationship between burial ages and incision is shown in Figure 5. For the four caves, we
225 observed a good relationship between burial ages and finite incision, except for the Camp-de-Guerre

226 cave (CDG) site, the higher the cave is, the older the burial ages are. Burial ages for the Cuillère
227 cave, Dugou cave, Camp-de-Guerre cave and Route cave are 2.16 ± 0.15 , 0.95 ± 0.14 , 0.63 ± 0.1 and
228 0.21 ± 0.1 Myrs respectively. This is consistent with the supposed cave evolution and first-order
229 constant incision of the Rieutord canyon. CDG age has to be considered with caution. The CDG cave
230 entrance located in a usually dry thalweg can act as a sinkhole or an overflowing spring depending on
231 the intensity of the rainfall. The sample was collected in a gallery showing evidence of active flooding
232 ~10 m above the Rieutord riverbed, therefore the older than expected age, given the elevation of the
233 cave, is probably due to cobbles that came from upper galleries during flood events. Forcing the linear
234 regression to go through the origin, leads to an incision rate of 83 ± 35 m/Ma. These results show that
235 at least half of the 300 m deep Rieutord Canyon is a Quaternary incision. Extrapolating the obtained
236 rate yields an age of 4.4 ± 1.9 Ma for the beginning of the canyon incision, which suggests that the
237 current landscape has been shaped during the Pliocene-Quaternary period. To extend our spatial
238 coverage and bring stronger confidence into our results, we combine Rieutord burial ages with
239 paleomagnetic data from watersheds located on the other side of the Hérault watershed.

240 **4.2.2. Local incision rate from paleomagnetic data (Southern Grands Causses)**

241 A total of 100 clay-infilling samples distributed over of 13 sites (i.e. profiles) was studied. The lowest
242 sample elevation above sea level (a.s.l.) is in the Garrel (ca 190 m) and the highest in the Leicasse (ca
243 580 m a.s.l.). In the Leicasse cave system, we sampled 8 profiles totalizing 60 samples. Profiles
244 elevations are located between ca 200 m and ca 400 m above the base level (a.b.l.), which corresponds
245 to the elevation of the Buèges river spring at 170 m a.s.l.

246 In the Garrel cave system, we sampled 5 profiles for a total of 40 samples that range between 20 m
247 and 80 m a.b.l. defined by the Garrel spring at 180 m a.s.l. Given the very marginal difference in
248 elevation between the local base levels from these two caves, we assume that they have the same local
249 base level. At each studied site, if all the profile samples have the same polarity, the site is granted
250 with the same polarity, either normal or reverse. If not (i.e. the profile displays normal and reverse
251 polarities), we consider it as a transitional site. Figure 6 shows the results plotted with respect to the
252 paleomagnetic scale (x axis) for the past 7 Ma, and their elevation above the base level (y axis). The
253 measured paleomagnetic polarities on each site is plotted several times for given incision rates
254 supposed to be constant through times (this allows determining different age models and analyze their
255 correlation with the distribution of paleomagnetic data, see below). First, we note a good agreement
256 between samples located at the same elevation and being part of the same stratigraphic layer
257 (Camus, 2003). This syngenetic deposition allows, as best explanation to prevent from a possible
258 partial endokarstic reworking. Second, the different elevations of the galleries where we collected the
259 samples allow proposing that the Leicasse deposits encompass at least three chrons, while the Garrel
260 deposits encompass only one. Third, a transitional signal comprised between a reversal signal (lower
261 samples) and a normal signal (upper ones) is observed at Les Gours sur Pattes (LGP) sampling site
262 (Fig. 7). This provides a strong constraint on the age of the sediment emplacement in the Leicasse

263 with respect to the magnetostratigraphic timescale (Fig. 6).
264 Compared to the Leicasse cave system, the elevation/polarity results for the Garrel are less
265 constrained. Only one site shows a reverse polarity at 90 m a.b.l., and the transitional polarity found at
266 40 m a.b.l. is unclear (tab, suppl mat.). The rest of the polarities (72 samples) are all normal. Given
267 that a U-Th ages younger than 90 kyrs was obtained for two speleothems (Camus, 2003) covering our
268 samples collected at 40 m a.b.l. (Fig. 6), we consider that the emplacement of the clay deposits
269 occurred during the most recent normal period and are therefore younger than 0.78 Ma (Figure 6).
270 The transition between the highest normal sample and the reversed one is located somewhere between
271 78 m and 93 m a.b.l. suggesting a maximum base level lowering rate of 109 ± 9 m/Ma.
272 To go further in the interpretation of our data, and better constraint the incision rate, we performed a
273 correlation analysis between observed and modeled polarities for a 0 to 200 m/Ma incision-rate range
274 (linear rate, each 1 m/Ma). Modeled polarities are found using the intersection between sample
275 elevation and incision-rate line.
276 We obtained 10 possible incision rates with the same best correlation factor (Fig. 8) spanning from 43
277 to 111 m/Ma (mean of 87 ± 24 m/Ma). Taking into account the transitional signal of the LGP site in
278 the Leicasse cave yields a linear incision rate of $83^{+17}_{-.5}$ m/Ma. Proposed uncertainties are based on
279 previous and next transition-related estimated incision rate.
280 Using a similar approach for the Rieutord crystalline samples, that is to say we compute, for the same
281 incision-rate space, the distance in a least square sens between the modeled age and the measured
282 ones in order to check the cost function shape and acuteness. With this method, we determined a
283 linear incision rate of 85 ± 11 m/Ma (Fig 8). Those two results, based on independent computations,
284 suggest the same first-order incision rate for the last 4 Ma of $84^{+21}_{-.12}$ m/Ma. Given that the Rieutord,
285 Garrel and Buèges rivers are all tributaries of the Hérault river, we propose that this rate represents the
286 incision rate for the Hérault river watershed, inducing approximately 300-350 m of finite incision over
287 the Pliocene-Quaternary period.
288 If the landscape is at first order in an equilibrium state, that is to say, if we preclude our incision rates
289 being a regressive erosional signal, the incision needs to be balanced by an equivalent amount of
290 uplift. If the uplift rate is roughly correlated to the regional topography, lowest uplift rates would be
291 expected in the south of our sampling sites inducing regional tilting of morphological benchmarks. In
292 the next part, we search for such evidences that would suggest differential uplift.

293

294 **5 Geomorphometric signature**

295

296 5.1 Tested hypothesis and methods

297 According to the Massif-Central centered uplift hypothesis, morphological markers such as strath
298 terraces, fluvio-karstic surfaces or abandoned meanders should display a southward tilting due to
299 differential uplift between the northern and the southern part of the region.

300 To investigate these differential vertical movement signals, we used the morphological markers
301 available in the study area (Fig. 9). We used a 5 m resolution DEM analysis to identify the markers
302 corresponding to surfaces with slope $< 2^\circ$. This cut-off slope angle prevents to identify surface related
303 to local deformation such as for example landslide or sinkhole. We point out that surface slope
304 increase through time (e.g. apparent tilting) could be due to diffusion processes and not related to
305 differential vertical displacements. However that problem is address by 1) the automatic selection and
306 correction and the final manual check for residue random distribution (see below).The local river
307 slope is on the order of 0.1° so the 2° cut-off angle is far from precluding to identify tilted markers.
308 We also use a criterion based on an altitudinal range for a surface. This altitudinal span is set
309 individually for each surface based on elevation, slope and curves map analysis, and encompass from
310 few meters to tens of meters depending on the size of the marker. We checked 80% of the identified
311 surfaces in the field in order to avoid misinterpretation. Some pictures are provided in supplementary
312 material. The dip direction and angle of the surface in computed in a two steps approach. First, we fit
313 a plan using extracted points from the DEM inside the delimited surface. Second, based on this plan
314 we remove the DEM points with residuals 3 times larger than the standard error and compute more
315 accurate plan parameters (second fitting). This outlier suppression removes any inaccurate DEM
316 points and correct for inaccurate surface delimitation (e.g. integration of a part of the edge of a strath
317 terrace, diffusion processes marks, etc.).
318 Because no obvious initially horizontal markers are known, we propose to correct the marker current
319 slope by the initial one to quantify the tilt since the marker emplacement. To do so we follow the
320 method used by Champagnac et al. (2008) for the Forealps. We identify the drain related to the marker
321 formation and compute its current local slope and direction. This method assumes that landscapes are
322 at the equilibrium state and that the river slope remained constant since the marker formation. This
323 assumption seems reasonable given the major river profiles and because most of the markers used are
324 far from the watershed high altitude areas precluding a recessive erosional signal. Finally, we
325 removed the local river plan from the DEM extracted surface.

326

327 5.2. Morphometrical results

328 Following this methodology, we obtained 61 surfaces (e.g. strath terraces). We then applied three
329 quality criterions to ensure the robustness of our results: 1) The minimal surface considered is 2500
330 m^2 based on a comparison between the 5m resolution DEM and a RTK GPS survey over 3 strath
331 terraces (Hérault river); 2) Final plans with dip angles larger than 2° are removed; 3) The residuals for
332 each geomorphological marker must be randomly distributed without marker edge signal, or clear
333 secondary structuration. Only 38 markers meet those 3 quality criterions.

334 If the identified and corrected markers have indeed registered a differential uplift between the north
335 and the south, we expected the following signals:

336 - The dipping direction of the tilted markers should be parallel to the main gradient of the topography,
337 i.e. between $150^\circ E$ and $180^\circ E$ for our studied region. This expectation is the most important one,
338 regarding uncertainties on the uplift rate and lithospheric elastic parameters.

339 - A latitudinal tilting trend, i.e. an increase of the tilt angle along the topography gradient. Indeed, null
340 or small tilts are expected near the shoreline and within the maximum uplift area of the
341 Cevennes/Massif Central, while the maximum tilt is expected at a mid-distance between these two
342 regions, i.e. about 50 km inland from the shoreline.

343 - A positive altitudinal tilting trend (an increase in dip angle with altitude). This trend would be
344 representative of the accumulation of finite tilt. However, it supposes a linear relationship between the
345 altitude and the age of the marker formation. If at first order, this straightforward hypothesis seems
346 reasonable for river-controlled markers (e.g. strath terraces), other surfaces are hardly expected to
347 follow such an easy relationship.

348

349 Among the three expected signal, southward dipping is robustly recorded with a mean tilt angle of
350 $0.60 \pm 0.40^\circ$ with an azimuth of $N128 \pm 36^\circ E$ (Fig. 10). Latitudinal trend and altitudinal trend are less
351 robustly reached but that is not surprising because of the strong susceptibility to local phenomenon or
352 even so lack of robust age constraint.

353

354 **6 Discussion**

355 Both geomorphological and geochronological evidence suggest a Pliocene-Quaternary uplift of the
356 Cevennes area. The origin of such uplift could be associated with several processes: erosion-induced
357 isostatic rebound, dynamic topography due to mantle convection, thermal isostasy, residual flexural
358 response due to the Gulf of Lion formation, etc. For the Alps and Pyrenees mountains, isostatic
359 adjustment due to erosion and glacial unloading has been recently quantified (Champagnac et al.,
360 2007, Vernant et al., 2013; Genti et al, 2016, Chery et al. 2016). Because the erosion rates measured in
361 the Cevennes are similar to those of the Eastern Pyrenees (Calvet et al., 2015, Sartégou et al., 2018a),
362 we investigate by numerical modeling how an erosion-induced isostatic rebound could impact the
363 southern Massif Central morphology and deformation.

364 We define a representative cross-section parallel to the main topographic gradient (i.e. NNW-SSE)
365 and close to the field investigation areas (Figure 11). We study the lithospheric elastic response to
366 erosion with the 2D finite element model ADELI (Hassani et Chery, 1996; Chéry et al. 2016). The
367 model is composed of a plate accounting for the elasticity of both crust and uppermost mantle.
368 Although the lithosphere rigidity of the European plate in southern Massif central is not precisely
369 known, vertical gradient temperatures provided by borehole measurements are consistent with heat
370 flow values ranging from 60 to 70 mW.m² (Lucazeau et Vasseur, 1989). Therefore, we investigate
371 plate thickness ranging from 10 to 50 km as done by Stewart et Watts (1997) for studying the vertical
372 motion of the alpine forelands.

373 We choose values for Young's and Poisson parameters of respectively 10^{11} Pa and 0.25, both
374 commonly used values for lithospheric modeling (e.g. Kooi et Cloething, 1992; Champagnac et al.

375 2007, Chéry et al., 2001). This leads to long-term rigidity of the lithosphere model ranging from 10^{21}
376 to 10^{25} N.m. Since the effect of mantle viscosity on elastic rebound is assumed to be negligible at the
377 time scale of our models (1 to 2 Myrs), we neglect the visco-elastic behaviour of the mantle.
378 Therefore, the base of the model is supported by an hydrostatic pressure boundary condition balancing
379 the weight of the lithosphere (Fig. 11). Horizontal displacements on vertical sides are set to zero since
380 geodetic measurements show no significant displacements (Nocquet et Calais, 2003; Nguyen et al.,
381 2016). The main parameters controlling our model are the erosion (or sedimentation) triggering
382 isostatic rebound and the elastic thickness.

383 The erosion profile (Fig. 11) is based on topography, our newly proposed incision rate and other
384 studies (Olivetti et al., 2016 for onshore denudation and Lofi et al., 2003; Leroux et al., 2014 for
385 offshore sedimentation). This profile is a simplification of the one that can be expected from Olivetti
386 et al. (2006) and do not aim at matching precisely the published data because of, (i) the explored time-
387 span (~ 1 Myrs) is not covered by thermochronological data (> 10 Myrs) or cosmogenic denudation
388 rate (10s-100s kyrs); (ii) we base our erosion rate as being linked with local (10 km²) slopes, that are
389 higher near the drainage divide. We, by this aim can invoke any kind of erosion processes (e.g.
390 landslides); and (iii) the model assumes a cylindrical structure and consequently, high-frequency
391 lateral variations in term of actual denudation rate or proxy (slope, elevation, etc.) must be averaged.
392 Concerning this erosion profile, parametric study (highest erosion rate ranging from 1 to 1000 m/Ma)
393 give no difference in the interpretation and, for few percent variations, only few percent variations in
394 the modeled uplift-rate.

395 The flexural rigidity controls the intensity and wavelength of the flexural response and ranges from
396 10^{21} to 10^{25} N.m. It can be expressed as a variation in elastic thickness (T_e) ranging from 4.4 to 96 km
397 (Fig. 12). We also test a possible T_e variation between inland and offshore areas. For the following
398 discussion, we use an elastic thickness of 15 km corresponding to a value of D of 3.75×10^{23} N/m. In
399 this case, the inland and offshore parts are largely decoupled and the large sedimentation rate in the
400 Gulf of Lion does not induce a flexural response on the Cévennes and Grands Causses areas.

401 With a maximum erosion rate of 80 m/Ma (Fig 11), the models display uplift rates of 50 m/Ma over
402 more than 100 km. As previously explained, the finite incision is permitted by an equal amount of
403 uplift considering that the incision is not due to regressive erosion.

404 Every models show a general uplift. However, the uplift amplitude are smaller than the expected ones.
405 To obtain the same uplift rate than the incision rates, the applied erosion rate over the model must be
406 increased. However, we assume that the landscape is at equilibrium, so, if the erosion rate is
407 increased, it will be higher than the incision rate leading to the decay of relief over the area. No
408 evidence of such evolution is found over the region and, if further studies need to be done to quantify
409 the actual erosion rate, we mostly think that a second process is acting, inducing the rest of the uplift
410 that can't be obtained by the erosion-induced isostatic adjustment. Finally, models predict a seaward

411 tilt of the surface at the regional-scale (Fig. 13), in agreement with the observed tilting of
412 morphological markers.

413 We assume that the sediments collected in the karst were deposited per descensum, i.e. we do not
414 know if the galleries existed a long time before or were formed just before the emplacement of the
415 sediments, but the more elevated the sediments are, the older their deposit is. If there is no evidence of
416 an important aggradation episode leading to more a complex evolution as proposed for the Ardèche
417 canyon (Moccochain et al., 2007; Tassy et al., 2013), we point out that small aggradation or null
418 erosion period could, however, be possible. Some processes could explain such relative stability: e.g.
419 variation in erosion (due to climatic fluctuation) or impact of eustatic variations (in river profile,
420 flexural response, etc.). Such transient variations have been shown for the Alps (Saillard et al., 2014;
421 Rolland et al., 2017) and are proposed as being related to climato-eustatic variations and therefore
422 should last 10 to 100 kyrs at most.

423 Based on our sampling resolution, we cannot evidence such transient periods and we must use an
424 average base level lowering rate in the karst, which we correlate to the incision of the main rivers. The
425 TCN-based incision rate derived from the Rieutord samples (83 ± 35 m/Ma) is consistent with the one
426 derived from the Garrel (U-Th ages: 85.83 m/Ma according to the sole U/Th exploitable result
427 (Camus, 2003)) and from the Garrel-Leicasse combination (Paleomagnetic approach: 84^{+21}_{-12} m/Ma).
428 This mean incision rate of ca. 85 m/Ma lasting at least 4 Ma, highlights the importance of the
429 Pliocene-Quaternary period into the Cévennes and Grand Causses morphogenesis. Furthermore, the
430 300 to 400 m of incision precludes a relative base level controlled by a sea-level drop. Indeed,
431 documented sea level variations are less than 100 m (Haq, 1988, Miller et al., 2005). Furthermore, the
432 Herault river does not show any significant knickpoints or evidence of unsteadiness in its profile as
433 expected if the incision was due to eustatic variations. Therefore, we propose that the incision rate of
434 ~ 85 m/Ma is due to a Pliocene-Quaternary uplift of the Cévennes and Grands Causses region.

435

436 Other river-valley processes could lead to a local apparent high incision rate as for instance major
437 landslide or alluvial fan (Ouimet et al., 2008). This hypothesis of an epigenetic formation of the
438 Rieutord is irrelevant because of i) none of the possible causes had been found in the Rieutord canyon
439 and ii) the consistency of the TCN-based incision rate and the paleomagnetic-based incision rate for
440 two other cave-systems. Indeed, the use of two independent approaches and three locations is a good
441 argument in favour of the robustness of our proposed mean 85 m/Ma incision rate. Yet, using more
442 data, particularly burial dating colocalized with clays samples and adding sampling sites would give a
443 stronger statistical validation. In the Lodève basin (Point 4, Fig. 1), inverted reliefs allow another
444 independent way to quantify minimal incision rate. K/Ar and paleomagnetic dated basaltic flows
445 spanning from 1 to 2 Myrs old that were deposited at the bottom of the former valley (Dautria et al.,
446 2010) are now located at ca 150 m above the current riverbed leading to an average incision rate of 77
447 ± 10 m/Ma, in agreement with karst-inferred incision rates.

448 Furthermore, preliminary results from canyons on the other side of the Grands Causses (Tarn and

449 Jonte) based on in-situ terrestrial cosmogenic dating suggest similar incision rates (Sartegou et al.,
450 2018b) and confirm a regional base level lowering of the Cévennes and Grands Causses region during
451 the Pliocene-Quaternary. This is consistent with the similarities of landscapes and lithologies observed
452 both on the Atlantic and Mediterranean watersheds (e.g. Tarn river).

453 Once the regional pattern of the Pliocene-Quaternary incision established for the Cévennes-Grands
454 Causses area, the next question is how this river downcutting is related to the regional uplift? First
455 order equilibrium shape and absence of major knick points in the main river profiles preclude the
456 hypothesis of regressive erosion. Hence, back to the three conceptual models presented in part 1
457 (Fig.2), we can discard, at first order, the models A (Old uplift-recent incision) and B (Old uplift-old
458 incision) because obtain incision rate show recent incision and surface tilting tend to prove a current
459 uplift. Therefore, the incision rate has to be balanced to the first order by the uplift rate. We add that
460 eustatic variations are of too low magnitude (100-120 m) and can't explain such total incision (up to
461 400m). Furthermore, no obvious evidence of active tectonics is reported for the area raising the
462 question of the processes responsible for this regional uplift. Very few denudation rates are reported
463 for our study area (Schaller et al., 2001; Molliex et al., 2016; Olivetti et al., 2017), and converting
464 canyon incision rates into denudation and erosion rates is not straightforward, especially given the
465 large karst developed in the area. Using a first order erosion/sedimentation profile following the main
466 topography gradient direction we have modeled the erosion-induced isostatic rebound. If this process
467 could create between half and two third of the Pliocene-Quaternary uplift, a previously existent
468 topography is needed to trigger erosion so it cannot explain neither the onset of the canyon-carving
469 nor the full uplift rates. Other, processes have to be explored such as dynamic topography or thermal
470 anomaly beneath the Massif-Central, the magmatism responsible for the important increase in
471 volcanic activity since ~ 6 Myrs (Michon et Merle, 2001; Nehlig et al., 2003) could play a major role,
472 notably in the initiation of Pliocene-Quaternary uplift. Further studies should aim to address the
473 problem of uplift onset, giving more clues concerning the stable continental area but owing the data
474 we presently have, discussing such onset is out of the scope of the paper.

475

476 7. Conclusion

477

478 Main results of this study are the following three points:

479 1- Mean incision rate of the Cevennes area is 83^{+17}_{-5} m/Ma during the last 4 Ma.

480 2- This incision is due to regional uplift with higher vertical velocities northward.

481 3- This uplift is partly due ($\frac{1}{2}$ to $\frac{2}{3}$) to isostatic adjustment induced by erosion.

482 Furthermore, our study highlights the importance of multidisciplinary approach especially in the study
483 of low-deformation rate areas.

484 To the contrary of previous studies that focused on one cave, we have shown that combining karst
485 burial ages and paleomagnetic analysis of clay deposits in several caves over a large elevation range
486 can bring good constraints on incision rates. This multi-cave system approach diminishes the intrinsic
487 limits of the two single methods: low sampling density (and analysis cost) for the TCN ages and

488 difficulty to set the position of paleomagnetic results. Our estimated paleo base level ages are
489 Pliocene-Quaternary (ca. last 4 Ma) and allow to derive a mean incision rate of 83^{+17}_{-5} m/Ma for the
490 Cévennes area. The landscape, and especially the river profiles suggest a first-order equilibrium
491 allowing considering the incision rate as an uplift rate.

492 We have shown using a geomorphological analysis that at least south of the Cévennes, several
493 surfaces are tilted toward the SSE. This kind of study had been performed before on large structures
494 (Champagnac et al., 2007) or endokarstic markers (Granger et Stock, 2004) but it is the first time that
495 it is performed at such scale with small markers. Numerical modeling yields the same pattern of SSE
496 dipping, allowing more confidence in the geomorphometric results.

497 Our multi-disciplinary approach brings the first absolute dating of the Cévennes landscapes and
498 suggests that the present-day morphology is partly inherited from the Plio-Quaternary erosion-
499 induced isostatic rebound.

500 We propose that related erosional isostatic adjustment is of major importance for the understanding of
501 the southern French Massif-Central landscape evolution and explains a large part of the uplift.

502 At larger scale, we assume that the main conclusion of our study can be extrapolated to the majority
503 of the intraplate orogens. That is to say, once the forces responsible for the initial uplift (e.g. plate
504 tectonics, dynamic topography) fade out, the uplift continue thanks to erosion-induced isostatic
505 adjustment.

506 An analysis at the scale of the Massif Central is now needed before nailing down our interpretations
507 of the Massif-Central dynamics.

508

509 **Code and data availability**

510 Surface analysis was performed using QGIS version 2.18, MATLAB® code and IGN DEM (RGE
511 Alti®) 5m). Modeling was performed using ADELI code (Hassani et Chery, 1996; Chéry et al., 2016).

512 Data for TCN and paleomagnetic analysis are provided in the manuscript itself or in supplementary
513 material. Additional informations for geologic background are available at <http://infoterre.brgm.fr/>
514 (French Geological Survey data visualizer).

515

516 **Author contributions**

517 OM, PV and GC did the sampling. GC and DF performed the TCN analysis. PC and OM did the
518 magnetic measurements and interpretations. OM did the surface identification and analysis. OM, PV
519 and JC performed the numerical model. OM, OV, JFR, GC, PC, JC and DF interpreted and wrote the
520 article.

521

522 **Competing interests**

523 The authors declare that they have no conflict of interest.

524

525 **Acknowledgments**

526 We are grateful to ANSTO for providing facilities for chemical extraction for the TCN analysis. We

527 thanks the reviewers for useful remarks and comments that we think help to increase the level of the
528 paper.

529 **References**

530

531 Arthaud F. et Laurent P.: Contraintes, déformations et déplacements dans l'avant-pays pyrénéen du
532 Languedoc méditerranéen, *Godin. Acta*, 8, 142-157, 1995.

533 Audra P., Camus H. et Rochette P.: Le karst des plateaux de la moyenne vallée de l'Ardèche : datation
534 par paléomagnétisme des phases d'évolution plio-quadernaires (aven de la Combe Rajeau). *Bull. Soc.*
535 *Géol. France*, 2001, t. 172. N°1, pp. 121-129, 2001.

536 Balco, G., Stone, J.O., Lifton, N.A., Dunai, T.J., 2008. A complete and easily accessible means of
537 calculating surface exposure ages or erosion rates from Be-10 and Al-26 measurements. *Quat.*
538 *Geochronol.* 3, 174–195. 2008.

539 Barbarand J., Lucazeau F., Pagel M. Et Séranne M.: Burial and exhumation history of the south-
540 eastern Massif Central (France) constrained by en apatite fission-track thermochronology.
541 *Tectonophysics*, 335, 275-290, 2001.

542 Barruol G. et Granet M.: A Tertiary astenospheric flow beneath the southern French Massif Central
543 indicated by upper mantle seismic anisotropy and related to the west Mediterranean extension. *Earth*
544 *and Planetary Science Letters* 202 (2002) 31-47, 2002.

545 Brichau S., Respaut J.P. et Monié P.: New age constraints on emplacement of the Cévenol granitoids,
546 South French Massif Central, *Int J Earth Sci* 97:725–738, doi: 10.1007/s00531-007-0187-x, 2007.

547 Bruxelles L.: Dépôts et altérites des plateaux du Larzac central : causes de l'Hospitalet et de
548 Campestre (Aveyron, Gard, Hérault) Evolution morphogénétique, conséquences géologiques et
549 implications pour l'aménagement. Université d'Aix-Marseille I, Université de Provence, UFR
550 Sciences géographiques et de l'aménagement. Thèse, spécialité : Milieux physiques méditerranéens,
551 2001.

552 Calais, E., Freed, A. M., Van Arsdale, R., & Stein, S. (2010). Triggering of New Madrid seismicity by
553 late-Pleistocene erosion. *Nature*, 466(7306), 608–611. <http://doi.org/10.1038/nature09258>

554 Calais, E., T. Camelbeeck, S. Stein, M. Liu, and T. J. Craig (2016), A new paradigm for large
555 earthquakes in stable continental plate interiors, *Geophys. Res. Lett.*, 43, doi:10.1002/2016GL070815,
556 2016.

557 Calvet M., Gunnell Y., Braucher R., Hez G., Bourlès D., Guillou V., Delmas M. et ASTER team: Cave
558 levels as proxies for measuring post-orogenic uplift : Evidence from cosmogenic dating of alluvium-
559 filled caves in the French Pyrenees. *Geomorphology* 246 (2015) 617- 633 ; doi :
560 10.1016/j.geomorph.2015.07.013, 2015.

561 Camus H.: Vallée et réseaux karstiques de la bordure carbonatée sud-cévenole. Relation avec la
562 surrection, le volcanisme et les paléoclimats. Thèse de doctorat, Université Bordeaux 3, 692 p, 2003.

563 Champagnac J.D., Molnar P., Anderson R.S., Sue C. et Delacou B.: Quaternary erosion-induced
564 isostatic rebound in the western Alps. *Geology*, March 2007 ; v.35 ; no. 3 ; p. 195-198, doi : 10.1130/
565 G23053A.1, 2007.

566 Champagnac J-D. van der Beek P. Diraison G. et Dauphin S.: Flexural isostatic response of the Alps
567 to increased Quaternary erosion recorded by foreland basin remnants, SE France. *Terra Nova*, Vol 20,
568 No. 3, 213-220, doi : 10.1111/j.1365-3121.2008.00809.x, 2008.

569 Chéry J., Zoback M.D. et Hassani R.: An integrated mechanical model of the San Andreas Fault in
570 central and northern California. *J. Geophys. Res.*, 106(B10) :22051. 52,61, 2001.

571 Chéry, J., Genti, M. And Vernant, P. Ice cap melting and low-viscosity crustal root explain the narrow
572 geodetic uplift of the Western Alps. *Geophys. Res. Lett.* 43,1–8 (2016).

573 Child D.P., Elliott G., Mifsud C., Smith A.M and Fink D., Sample processing for earth science studies
574 at ANTARES. *Nuclear Instruments and Methods in Physics Research Section B Beam Interactions*
575 *with Materials and Atoms* 172(1-4):856-860 doi: 10.1016/S0168-583X(00)00198-1, 2000.

576 Corbel J.: Les phénomènes karstiques dans les Grands Causses. In : *Revue de géographie de Lyon*,
577 vol. 29, n°4, pp. 287-315, doi : 10.3406/geoca.1954.1990, 1954.

578 Dautria J.M., Liotard J.M., Bosch D., Alard O.: 160 Ma of sporadic basaltic activity on the Languedoc
579 volcanic line (Southern France): A peculiar cas of lithosphere-asthenosphere interplay. *Lithos* 120
580 (2010) 202-222, doi: 10.1016/j.lithos.2010.04.009, 2010

581 Genti M.: Impact des processus de surface sur la déformation actuelle des Pyrénées et des Alpes.
582 *Géophysique [physics.geo-ph]*. Université de Montpellier, 2015. Français. Thèse, 2016.

583 Granet M., Wilson M. et Achauer U.: Imaging a mantle plume beneath the French Massif Central.
584 *Earth and Planetary Science Letters* 136 (1995) 281-296, 1995.

585 Granger, D. E., Fabel, D. and Palmer, A.N.: Pliocene-Pleistocene incision of the Green River,
586 Kentucky determined from radioactive decay of comogenic ²⁶Al and ¹⁰Be in Mammoth Cave
587 sediments. *GSA Bulletin*; July 2001; v. 113; no. 7; p. 825–836

588 Granger, D. E., Kirchner, J. W., and Finkel, R. C.: Quaternary downcutting rate of the New River,
589 Virginia, measured from differential decay of cosmogenic ²⁶Al and ¹⁰Be in cave-deposited alluvium.
590 *Geology*; February 1997 ; v. 25 ; no.2 ; p. 107-110, 1997.

591 Granger D.E., Gibbon R.J., Kuman K., Clarke R.J., Bruxelles L. and Caffee M.W.: New cosmogenic
592 burial ages for Sterkfontein Member 2 Australopithecus and Member 5 Oldowan, *Nature Letter* 2015,
593 doi: 10.1038/nature14268, 2015.

594 Granger D.E. and Muzikar P.F.: Dating sediment burial with in situ-produced cosmogenic nuclides:
595 theory, techniques, and limitations. *Earth and Planetary Science Letters* 188 (2001) 269-281, 2001.

596 Granger D.E. and Stock G.M.: Using cave deposits as geologic tiltmeters : Application to postglacial
597 rebound of the Sierra Nevada, California. *Geophysical Research Letters*, vol. 31, L22501, doi :
598 10.1029/2004GL021403, 2004.

599 Zupan Hajna N., Mihevc A., Pruner P. and Bosák P. 2010. Palaeomagnetic research on karst sediments
600 in Slovenia. *International Journal of Speleology*, 39(2), 47-60. Bologna (Italy). ISSN 0392-6672,
601 2010.

602 Haq B.U., Herdenbol J. and Vail P.R.: Mesozoic and cenozoic chronostratigraphy and cycles of sea-
603 level change. Society Economic Paleontologists Mineralogists Special Publication, 42, 71-108, Tulsa,
604 Oklahoma. 1988.

605 Harmand D., Adamson K., Rixhon G., Jaillet S., Losson B., Devos A., Hez G., Calvet M. and Audra
606 P.: Relationships between fluvial evolution and karstification related to climatic, tectonic and eustatic
607 forcing in temperate regions, *Quaternary Science Reviews* (2017) 1-19, doi :
608 10.1016/j.quascirev.2017.02.016, 2017.

609 Hassani R. and Chery J., Anelasticity explains topography associated with Basin and Range normal
610 faulting. *Geology* 24(12):1095. doi: 10.1130/0091-7613(1996)024<1095:AETAWB>2.3.CO;2. 1996.

611 Hill C.A., 1999.. Sedimentology and Paleomagnetism of sediments, Kartchner caverns, Arizona.
612 *Journal of Cave and Karst Studies* 61(2) : 79-83, 1999.

613 Husson E.: Intéraction géodynamique/karstification et modélisation 3D des massifs carbonatés :
614 Implication sur la distribution prévisionnelle de la karstification. Exemple des paléokarsts créacés à
615 néogènes du Languedoc montpelliérain. *Sciences de la Terre. Université Montpellier 2- Sciences et*
616 *techniques du Languedoc*, 236 p, 2014.

617 Kooi H., Cloetingh S. et Burrus J.: Lithospheric Necking and Regional Isostasy at Extensional Basins
618 1. Subsidence and Gravity Modeling With an Application to the Gulf of Lions Margin (SE France),
619 *Journal of Geophysical Research* , vol. 97, no. B12, Pages 17,553- 17,571, november 10, 1992.

620 Leroux E., Rabineau M., Aslanian D., Granjeon D., Droz L. et Gorini C.: Stratigraphic simulations of
621 the shelf of the Gulf of Lions: testing subsidence rates and sea-level curves during the Pliocene and
622 Quaternary. *Terra Nova*, Vol 26, No. 3, 230-238, doi: 10.1111/ter.12091, 2014.

623 Lofi J., Rabineau M., Gorini C., Berne S., Clauzon G., De Clarens P., Dos Reis A.T., Mountain G.S.,
624 Ryan W.B.F, Steckler M.S. et Fouchet C.: Plio-Quaternary prograding clinoform wedges of the
625 western Gulf of Lion continental margin (NW Mediterranean) after the Messinian Salinity Crisis.,
626 *Marine Geology* July 2003; 198 (3-4) : 289-317, doi: 10.1016/S0025-3227(03)00120-8, 2003.

627 Lucazeau F. and Vasseur G.: Heat flow density data from France and surrounding margins, In: V.
628 Cermak, L. Rybach and E.R. Decker (Editors), *Tectonophysics*, 164 (1989) 251-258

629 Manchuel K., Traversa P., Baumont D., Cara M., Nayman E. Et Durouchoux C.: The French seismic
630 CATalogue (FCAT-17), *Bull Earthquake Eng* (2018) 16:2227–2251, doi: 10.1007/s10518-017-0236-1,
631 2018.

632 Miallier D., Michon L., Evin J., Pilleyre T., Sanzelle S., et Vernet G.: Volcans de la Chaîne des Puys
633 (Massif Central, France) : point sur la chronologie Vasset-Kilian-Pariou-Chopine. *Comptes Rendus*
634 *Géoscience*, Elsevier

635 Michon L. et Merle O.: The evolution of the Massif Central rift: Spatio-temporal distribution of the
636 volcanism. *Bulletin de la Society Geologique de France*, 2001, t. 172, n°2, pp. 201-211, dog:
637 102113/172.2.201, 2001.

638 Miller, K.G., Kominz, M.A., Browning, J.V., Wright, J.D., Mountain, G.S., Katz, M.E., Sugarman,
639 P.J., Cramer, B.S., Christie-Blick, N., Pekar, S.F.: The Phanerozoic record of global sea-level change.
640 *Science* 310, 1293–1298, doi : 10.1126/science.1116412, 2005.

641 Mocochain L.: Les manifestations géodynamiques –Externes et internes- de la crise de salinité
642 messinienne sur une plate-forme carbonatée peri-méditerranéenne : le karst de la basse ardèche
643 (moyenne vallée du Rhône ; France). Thèse de doctorat, Université Aix- Marseille I – Université de
644 Provence U.F.R des Sciences géographiques et de l'aménagement Centre Européen de Recherches et
645 d'Enseignement en Géosciences de l'Environnement., 196 p, 2007.

646 Molliex S., Rabineau M., Leroux E., Bourlès D.L., Authemayou C., Aslanian D., Chauvet F., Civet F.
647 et Jouët G.: Multi-approach quantification of denudation rates in the Gulf of Lion source-to-sink
648 system (SE-France). *Earth and Planetary Science Letters* 444 (2016) 101-115, doi :
649 10.1016/j.epsl.2016.03.043, 2016.

650 Nehlig P., Boivin P., de Goër A., Mergoïl J., Prouteau G., Sustrac G. Et Thiéblemont D.: Les volcans
651 du Massif central. *Revue BRGM: Géologues, Numéro Spécial: Massif central*, 2003.

652 Nguyen H. N., Vernant P., Mazzotti S., Khazaradze G. et Asensio E.: 3-D GPS velocity field and its
653 implications on the present-day post-orogenic deformation of the Western Alps and Pyrenees. *Solid*
654 *Earth*, 7 ; 1349-1363, 2016, doi : 10.5194/se-7-1349-2016, 2016.

655 Nocquet J.-M. et Calais E.: Crustal velocity field of western Europe from permanent GPS array
656 solutions, 1996-2001. *Geophys. J. Int.* (2003) 154, 72-88, doi : 10.1046/j.1365-246X.2003.01935.x,
657 2003.

658 Nocquet J.-M., Sue C., Walpersdorf A., Tran T., Lenôtre N., Vernant P., Cushing M., Jouanne F.,
659 Masson F., Baize S., Chéry J. and Van der Beek P.A., Present-day uplift of the western Alps, *Sci. Rep.*
660 6, 28404; doi: 10.1038/srep28404 (2016).

661 Olivetti V., Godard V., Bellier O. et ASTER team : Cenozoic rejuvenation events of Massif Central
662 topography (France) : Insights from cosmogenic denudation rates and river profiles. *Earth and*
663 *Planetary Science Letters* 444 (2016) 179-191, doi : 10.1016/j.epsl.2016.03.049 0012-821X, 2016.

664 Ouimet, WB, Whipple, KX, Crosby, BT, Johnson, JP, Schildgen, TF. 2008. Epigenetic gorges in
665 fluvial landscapes. *Earth Surface Processes and Landforms* 33: 1993– 2009. doi: 10.1002/esp.1650
666 Epigenetic. 2008.

667 Rolland Y., Petit C., Saillard M., Braucher R., Bourlès D., Darnault R. Cassol D. Et ASTER Team:
668 Inner gorges incision history: A proxy for deglaciation? Insights from Cosmic Ray Exposure dating
669 (¹⁰Be and ³⁶Cl) of river-polished surfaces (Tinée River, SW Alps, France). *Earth and Planetary*
670 *Science Letters*, Elsevier, 2017, 457, pp.271 - 281, doi : 10.1016/j.epsl.2016.10.007. <hal-01420882>,
671 2017.

672 Rovey II C.W., Balco G., Forir M. Et Kean W.F.: Stratigraphy, paleomagnetism, and cosmogenic-
673 isotope burial ages of fossil-bearing strata within Riverbluff Cave, Greene County, Missouri.
674 *Quaternary Research* (2017), 1-13, doi : 10.1017/qua.2017.14, 2017.

675 Saillard M., Petit C., Rolland Y., Braucher R., BOurlès D.L., Zerathe S., Revel M. Et Jourdon A.: Late
676 Quaternary incision rates in the Vésubie catchment area (Southern French Alps) from in situ-produced
677 ³⁶Cl cosmogenic nuclide dating: Tectonic and climatic implications, *J. Geophys. Res. Earth Surf.*, 119,
678 1121–1135, doi:10.1002/ 2013JF002985. 2014.

679 Sanchis E. et Séranne M.: Structural style and tectonic evolution of a polyphase extensional basin of
680 the Gulf of Lion passive margin : the Tertiary Alès basin, southern France. *Tectonophysics* 322 (2000)
681 219-242, doi : 10.1016/S0040-1951(00)00097-4, 2000.

682 Sartégou A.: Évolution morphogénique des Pyrénées orientales: apports des datations de systèmes
683 karstiques étagés par les nucléides cosmogéniques et la RPE. *Géomorphologie*. Thèse de l'Université
684 de Perpignan. Français <NNT : 2017PERP0044>. <tel-01708921> , 2017.

685 Sartégou, A., Boulès, D. L., Blard, P.-H., Braucher, R., Tibari, B., Zimmermann, L., et al. (2018a).
686 Deciphering landscape evolution with karstic networks_ A Pyrenean case study. *Quaternary*
687 *Geochronology*, 43, 12–29. <http://doi.org/10.1016/j.quageo.2017.09.005>

688 Sartégou A., Mialon A., Thomas S., Giordani A., Lacour Q., Jacquet A., André D., Calmels L.,
689 Boulès D.L., Bruxelles L., Braucher R., Leanni L. Et ASTER team.: When TCN meet high school
690 students: deciphering western Cévennes landscape evolution (Lozère, France) sin g TCN on karstic
691 networks. Poster 4th Nordic Workshop on Cosmogenic Nuclides. 2018b.

692 Schaller M., von Blanckenburg F., Hovius N. Et Kubik P.W.: Large-scale erosion rates from in situ-
693 produced cosmogenic nuclides in European river sediments. *Earth and Planetary Science Letters* 188
694 (2001) 441-458, 2001.

695 Séranne M., Benedicto A., Labaum P., Truffert C. et Pascal G.: Structural style and evolution of the
696 Gulf of Lion Oligo-Miocene rifting : role of the Pyrenean orogeny. *Marine and Petroleum Geology*,
697 Vol. 12, No. 8, pp. 809-820, 1995.

698 Séranne M., Camus H., Lucazeau F., Barbarand J. et Quinif Y.: Surrection et érosion polyphasées de la
699 Bordure cévenole. Un exemple de morphogenèse lente. *Bull. Soc. Géol. France*, 2002, t. 173, n°2, pp.
700 97-112, 2002.

701 Sibuet J.-C., Srivastava S.P. et Spakman W.: Pyrenean orogeny and plate kinematics. *Journal of*
702 *Geophysical Research: Solid Earth*, Vol 109, doi: 10.1029/2003JB002514 , 2004.

703 Spassov S. et Valet J.-P.: Detrital magnetisations from redeposition experiments of different natural
704 sediments. *Earth and Planetary Science Letters* 351-352 (2012) 147-157, doi:
705 10.1016/j.epsl.2012.07.016, 2012

706 Stewart J. and Watts A.B.: Gravity anomalies and spatial variation of flexural rigidity at mountain
707 ranges. *Journal of Geophysical research*, vol 102, no. B3, Pages 5327-5352, march 10, 1997, doi:
708 10.1029/96JB03664, 1997.

709 Stock G.M., Granger D.E., Sasowsky I.D., Anderson R.S. et Finkel R.C.: Comparison of U-Th,
710 paleomagnetism, and cosmogenic burial methods for dating caves : Implications for landscape
711 evolution studies. *Earth en Planetary Science Letters* 236 (2005) 388-403, doi :
712 10.1016/j.epsl.2005.04.024, 2005.

713 Tarayoun A., Mazzotti S., Gueydan F., Quantitative impact of structural inheritance on present-day
714 deformation and seismicity concentration in intraplate deformation zones, *Earth and Planetary*
715 *Science Letters*, Volume 518, 2019, Pages 160-171, ISSN 0012-821X, doi:
716 10.1016/j.epsl.2019.04.043., 2017.

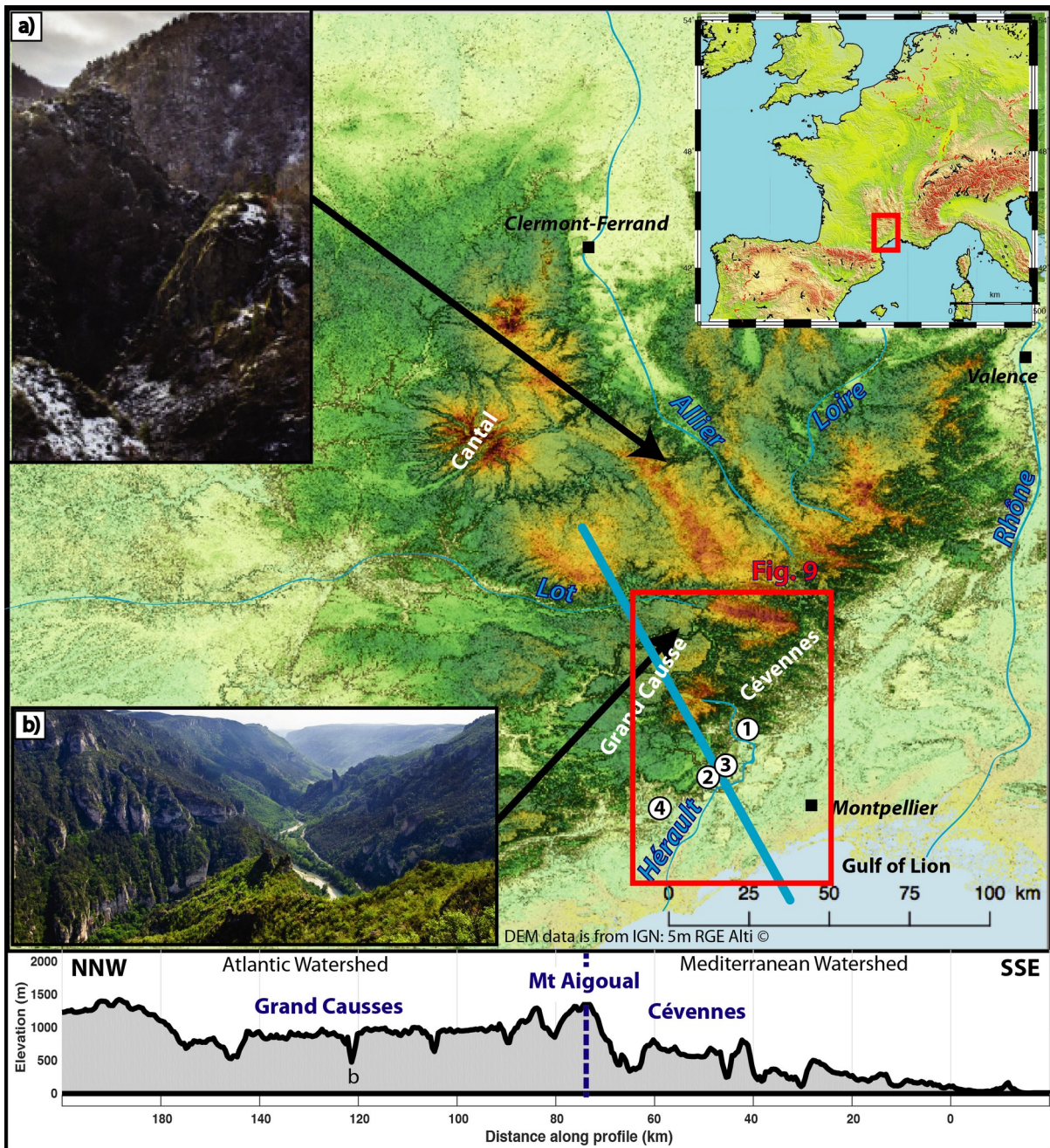
717 Tassy A., Mocochain L., Bellier O., Braucher R., Gattacceca J., Bourlès D.: Coupling cosmogenic
718 dating and magnetostratigraphy to constrain the chronological evolution of peri-Mediterranean karsts
719 during the Messinian and the Pliocene: Example of Ardèche Valley, Southern France. *Geomorphology*,
720 189 (2013), pp. 81-92, doi: 10.1016/j.geomorph.2013.01.019, 2013.

721 Tauxe L., Steindorf J.L. et Harris A.: Depositional remanent magnetisation: Toward an improved
722 theoretical and experimental foundation. *Earth and Planetary Science Letters* 244 (2006) 515-529, doi:
723 10.1016/J.epsl.2006.02.003, 2006.

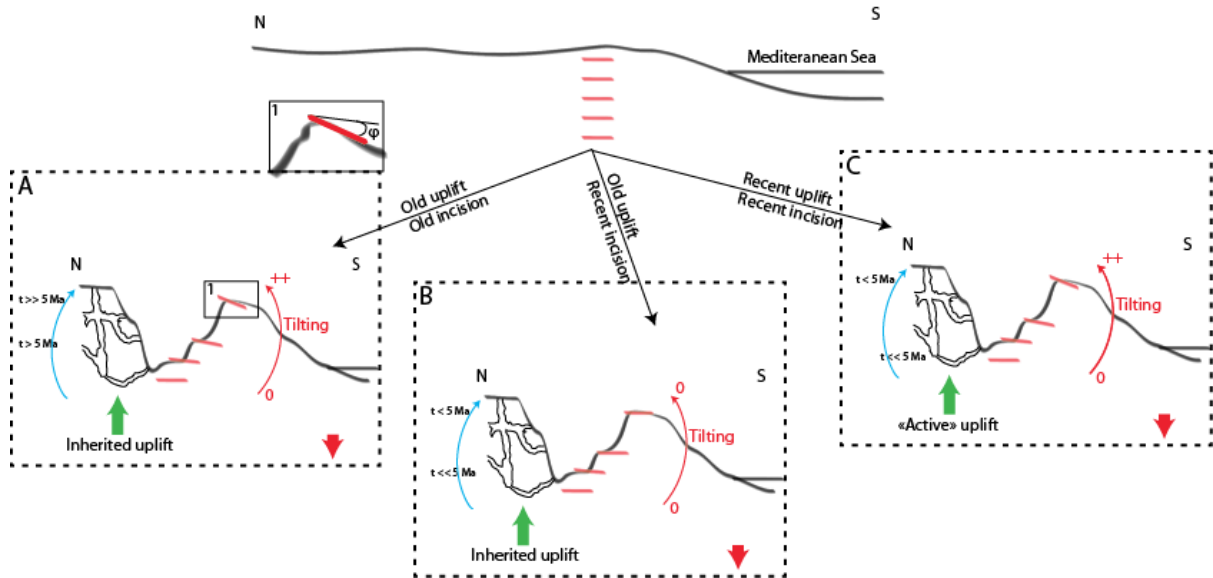
724 Tricart P. : From passive margin to continental collision: A tectonic scenario for the western Alps.
725 *American journal of science*, Vol. 284, February, 1984, P97-120, 1984.

726 Vernant, P., Hivert, F., Chéry, J., Steer, P., Cattin, R., & Rigo, A. (2013). Erosion-induced isostatic
727 rebound triggers extension in low convergent mountain ranges. *Geology*, 41(4), 467–470.
728 <http://doi.org/10.1130/G33942.1>

729
730
731
732
733
734



735
 736 **Figure 1: 30 m resolution DEM of the French Massif-Central and slope shadowed. Examples of finite**
 737 **incision typical of the French Massif-Central in a) crystalline basement (Seuge Canyon) and b)**
 738 **limestone plateau (Tarn Canyon). Location of the study area in red box (Fig. 9) and numerated site**
 739 **1) is the Rieutord Canyon (43,958°N; 3.709°E) where TCN measurements have been done, 2) and 3)**
 740 **are the Leicasse Cave System (43,819°N; 3.56°E), and the Garrel Cave system (43,835°N; 3.616°E)**
 741 **respectively, where paleomagnetic analysis have been done and 4) is the Lodève basin (43,669°N;**
 742 **3.382°E) with dated basaltic flows. Bottom panel is an example of typical topographic profile used**
 743 **for the numerical model set up.**
 744 **Note the south-western area with large plateau dissected by canyon, and the rugged area with**
 745 **steep valley called the Cevenne. They are typical regional limestone and crystalline morphology**
 746 **respectively.**



747
748
749
750
751
752
753
754
755
756

Figure 2: conceptual models for landscape evolution. Top panel is the initial stage (prior to uplift). Each panel represents a possible scenario explaining current morphology: A) Old uplift and old incision, B) Old uplift and recent incision and C) both recent uplift and incision. Blue arrow and associated ages show expected result (or absence of) for burial dating. Red level represents morphological markers that are fossilised when reaching the surface, accumulating afterward (or not) the differential uplift by finite tilting.



757
758
759
760
761
762
763
764

Figure 3: Example of quartz cobbles sampled for burial dating. Location: Cuillère Cave (Site 1, Fig.1)

765

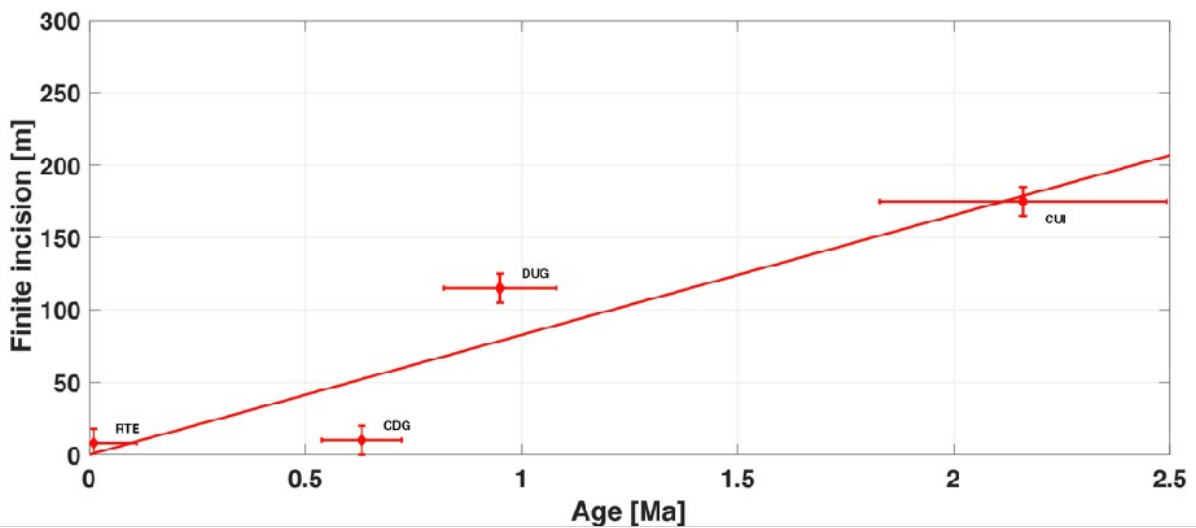


766

767 **Figure 4: Example of clay sampling for the paleomagnetic study. Location at the entrance shaft (Highest**
768 **elevation of every samples (~580 m a.s.l.), Leicasse Cave system, Site 2, Fig. 1)**

769

770



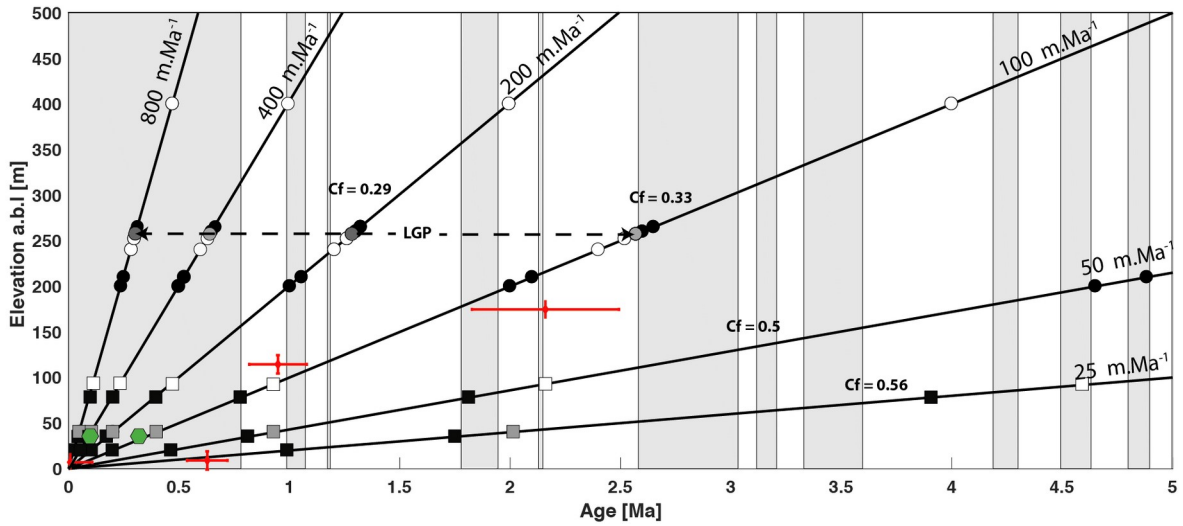
771

772 **Figure 5: Correlation diagram of finite incision and burial age for the Rieutord canyon (Site 1, Fig.**
773 **1). Finite incision is the elevation of the sampling site relatively to the current riverbed. RTE for**
774 **Route Cave, CDG for Camp de Guerre Cave, DUG for Dugou Cave and CUI for Cuillère Cave**

775

776

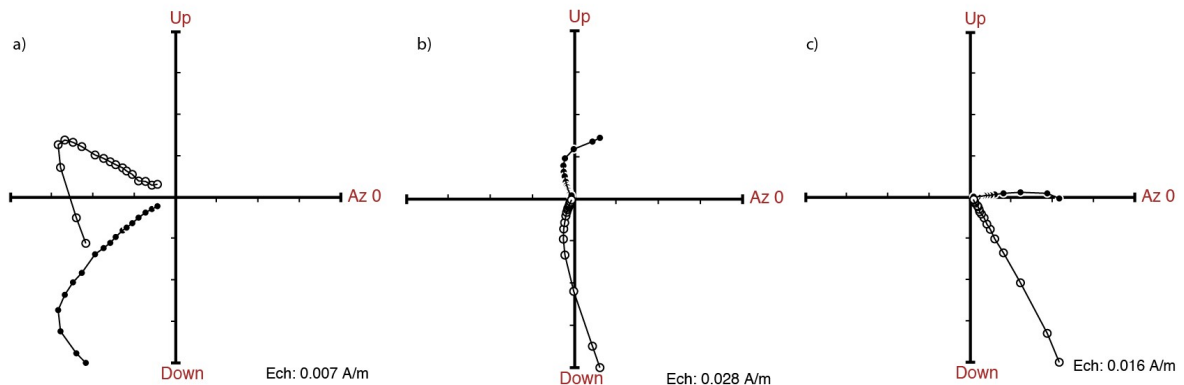
777



778
 779 Figure 6. Constraining the incision rate in the Cevennes margin, using paleomagnetic polarities from
 780 clay deposits (black, grey and white symbols) and burial ages (red crosses): Circles are from the Le-
 781 icasse cave with LGP being *les gours sur pattes* profile (see text), squares are from the Garrel cave.
 782 Black, grey and white symbols correspond to normal, transitional and reverse polarities, respectively.
 783 Black linear straight lines define possible incision rates that are supposed stable thought time. (num-
 784 bers in white rectangles define the Cf values are correlation factor between the measured paleomag-
 785 netic polarities and the predicted paleomagnetic scale (see also Figure 8). Green hexagons show the
 786 U/Th ages obtained on speleothems in the Garrel by Camus (2003).

787

788

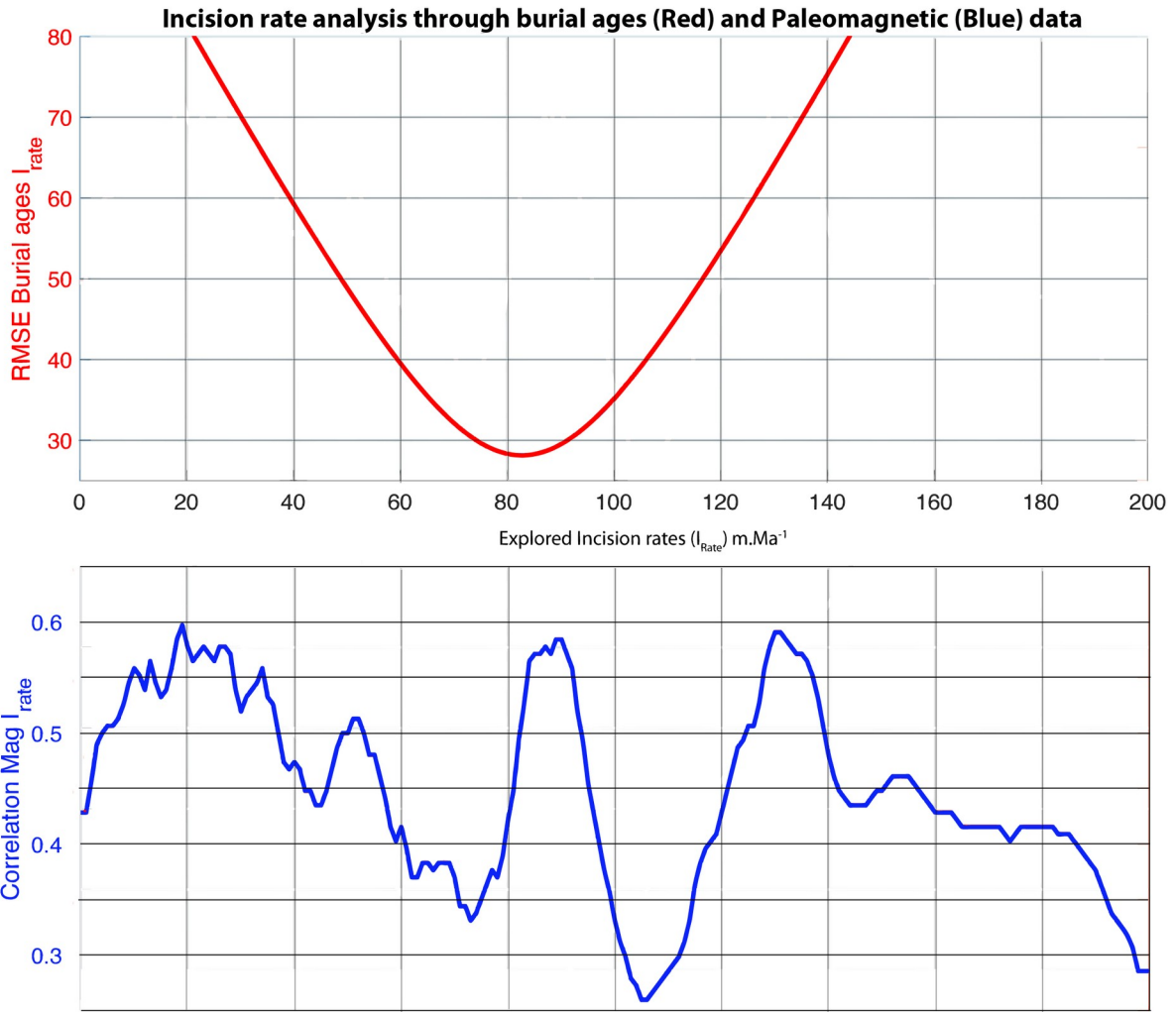


789

790

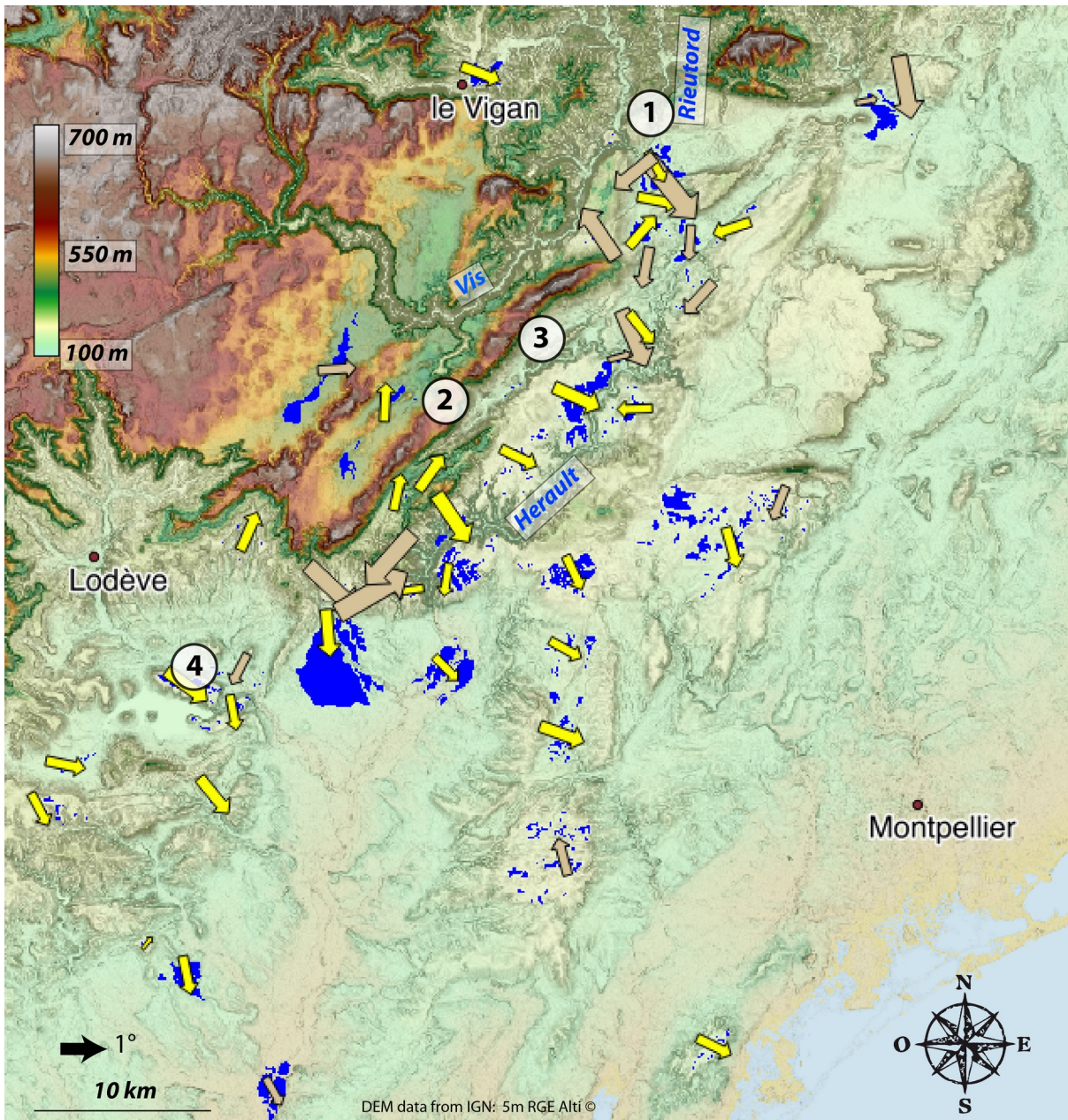
791

792 **Figure 7: Zijderveld Diagram for three samples from the Gours-sur-Pattes (Leicasse, Site 2,**
 793 **Fig.1) site. Stratigraphical order is from a) (the older, base of the profile) to c) (the younger, top**
 794 **of the profile).**



795
 796 **Figure 8: Best incision rates based on paleomagnetic data (blue) and burial ages (red). The blue**
 797 **curve is the normalized smoothed (10 m/Ma sliding window for better visualization) correlation**
 798 **between theoretical and observed polarities. The highest correlation corresponds to the best**
 799 **incision rates. The red curve is the RMSE for the linear regression through the burial ages data set**
 800 **shown on Fig. 4.**

801
 802
 803
 804
 805
 806
 807
 808
 809
 810
 811
 812
 813



814

815

816 **Figure 9: Tilting map of geomorphological benchmark (blue areas). Base-map is 30 m resolution**
 817 **DEM with slope shadow. Arrows are orientated according to the marker downward dip. The arrow**
 818 **size is set accordingly to the corrected tilting angle (the bigger, the more the tilting). Yellow and**
 819 **brown arrows are for robust and less robust surfaces respectively. Several arrows are hidden**
 820 **because of their small size and too high proximity with bigger ones. Numerated site 1) is the**
 821 **Rieutord Canyon, 2) is the Leicasse Cave System, 3) is the Garrel Cave system and 4) is the Lodève**
 822 **basin with dated basaltic flows. See Fig. 1 for geographical coordinates.**

823

824

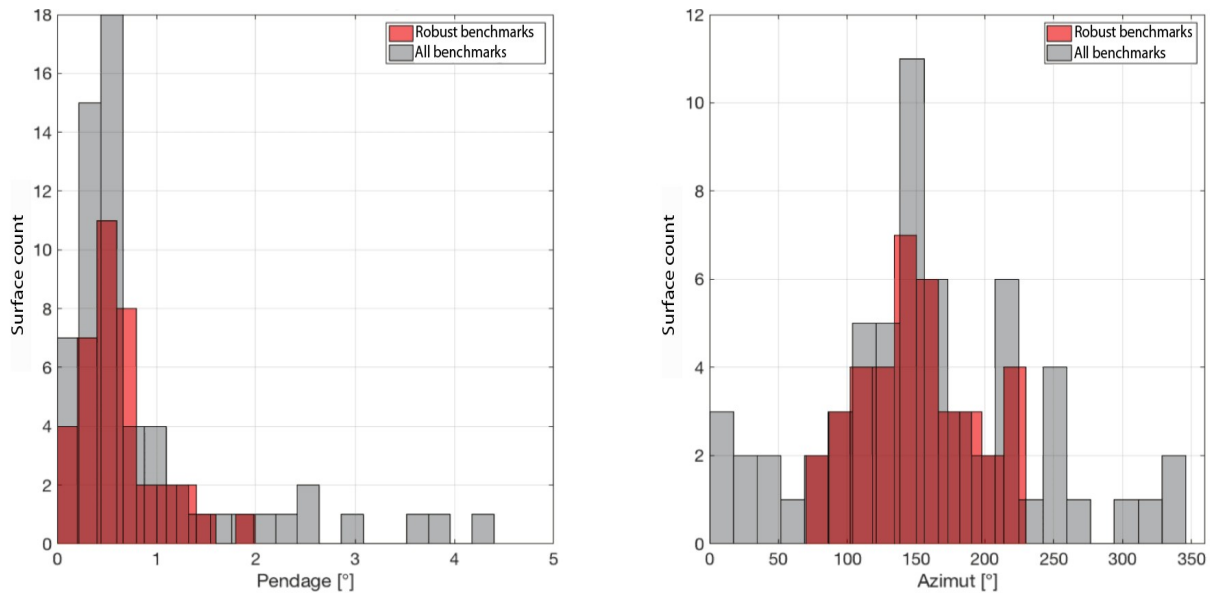
825

826

827

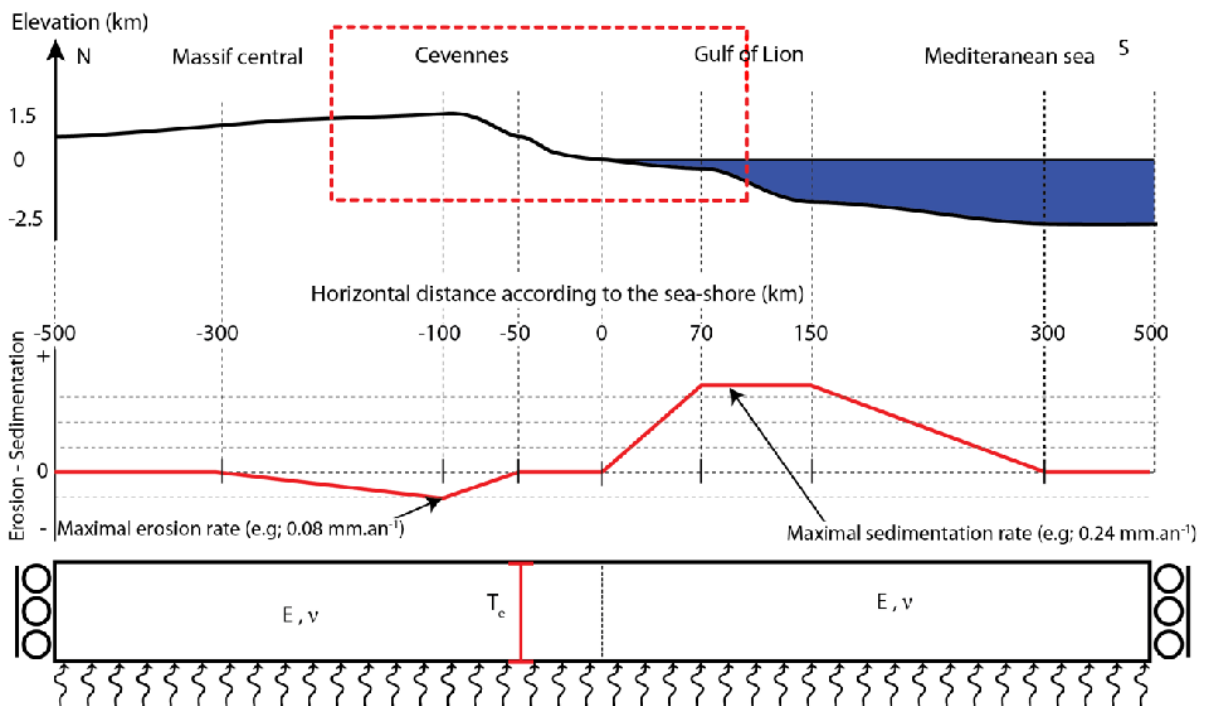
828

829



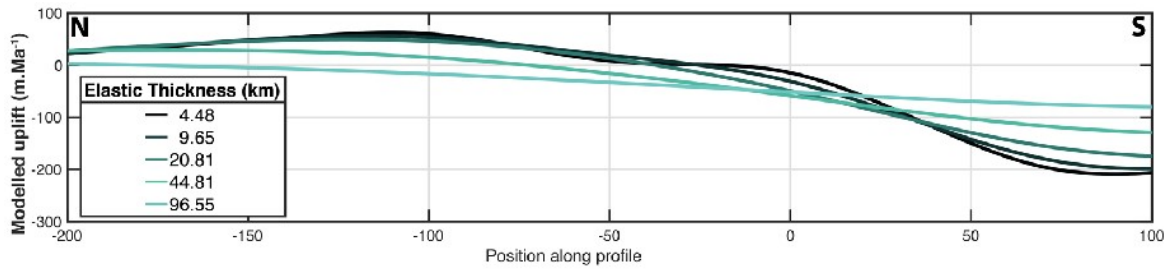
830
 831 **Figure 10: Tilting and azimuth distribution.** Left panel is density distribution for surface maximum
 832 **tilting in degree.** Right panel is azimuth of maximum dipping relative to the north. For each
 833 **histogram, red and grey populations are for robust and primary detected markers.**

834
 835
 836

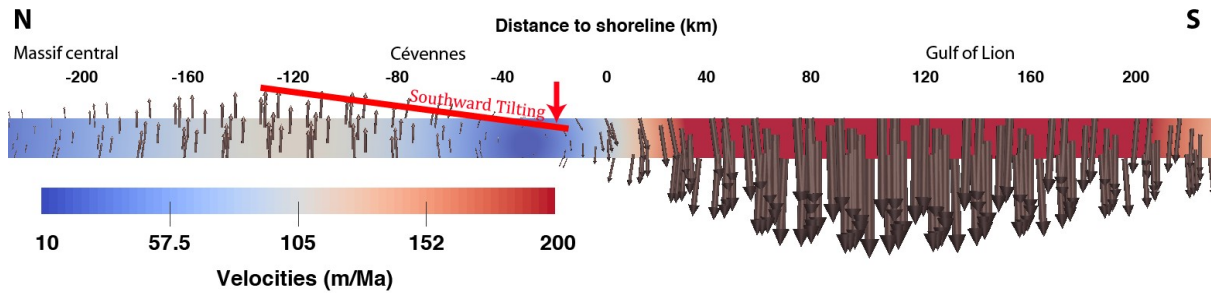


837
 838
 839
 840 **Figure 11: Top panel: schematic topographic profile.** The red box delimits the area shown Fig. 1
 841 **and 9.** Middle panel, surface processes profile, negative values are for erosion and positive values
 842 **for sedimentation.** Bottom panel: model set-up with two compartments (one for the Cevennes area
 843 **and the second one for the gulf of Lion).** The base of the model is compensated in pressure and the
 844 **right and left limits are fixed at zero horizontal velocity and free vertical velocity.** T_c is the
 845 **equivalent elastic thickness (in km), E (Pa) and ν are the Young modulus and the Poisson**
 846 **coefficient respectively whom values are independent in each compartment.**

847



849 **Figure 12: Modeled uplift according to different Te. Most plausible Te are between 10 and 30 km.**



851 **Figure 13: Modeling result for Te= 15 km. Erosion-sedimentation rate profile is the same as in Fig.**
 852 **6. Velocity field is shown using arrow for orientation velocity magnitudes are quantified by the**
 853 **font color code. Black values on top are distance relative to the sea-shore (positive value landward**
 854 **and negative values seaward). Red line represents the southward modeled tilting due to**
 855 **differential uplift.**

856

Cave	Lat	Lon	Elevation	Height	Conc ¹⁰ Be (10 ⁴ atm/g)	σ ¹⁰ Be (10 ³ atm/g)	Conc ²⁶ Al (10 ⁵ atm/g)	σ ²⁶ Al (10 ⁴ atm/g)	²⁶ Al/ ¹⁰ Be (and σ)	Burial age and σ (Ma)
RTE	43.960	3.707	175	8	3.54	1.18	2.16	1.47	6.11 ± 0.46	0.20 ± 0.15
CDG	43.955	3.710	185	10	8.87	3.12	4.29	3.28	4.83 ± 0.41	0.67 ± 0.16
DUG	43.957	3.711	245	115	1.27	5.68	0.529	0.636	4.15 ± 0.53	0.99 ± 0.25
CUI	43.959	3.711	354	175	1.70	7.14	0.375	0.528	2.20 ± 0.32	2.28 ± 0.28

857

858 Table 1: Samples analytical results and parameters. Cave code are: RTE for the “de la route” Cave, CDG for the
 859 “Camp de Guerre” cave, DUG for the “Dugou” Cave and CUI for the “Cuillère” Cave. Main parameters are the
 860 geographical coordinate (Lat, Lon in decimals degree), the elevation (a.s.l), the height (a.b.l., computed
 861 relatively to the surface river elevation. The concentration (atoms/g quartz) of ¹⁰Be and ²⁶Al in collected sand
 862 samples are all AMS ¹⁰Be/Be and ²⁶Al/Al isotopic ratios corrected for full procedural chemistry blanks and
 863 normalized to KN-5-4 and KN -4-2, respectively. The error in the brackets is for total analytical error in final
 864 average ¹⁰Be and ²⁶Al concentrations based on statistical counting errors in final ¹⁰Be/Be (²⁶Al/Al) ratios
 865 measured by AMS in quadrature with a 1% error in ⁹Be spike concentration (or a 4% error in ²⁷Al assay in
 866 quartz) and a 2% (or 3%) reproducibility error based on repeat of AMS standards. Burial age (minimum)
 867 assuming no post-burial production by muons at given depth (all deeper than 30m) in cave below surface and
 868 assuming initial ²⁶Al/¹⁰Be ratio is given by the production ratio of 6.75. The burial age error determined by using
 869 a +/-1σ range in the measured ²⁶Al/¹⁰Be ratio